JOURNAL OF GUIDANCE, CONTROL, AND DYNAMICS
Vol. 34, No. 2, March–April 2011

Practical Stochastic Optimal Guidance Law for Bounded Acceleration Missiles

G. Hexner*
Rafael, Haifa, 31021 Israel
and
A. W. Pila†
Israel Military Industries, Ltd., Ramat HaSharon, 47100 Israel

DOI: 10.2514/1.51543

The purpose of this paper is to develop an optimal guidance law that takes into account both the missile acceleration limit and a maximum value allowed for the guidance gain. The maximum value of the guidance gain is dictated mainly by the possible coupling between the missile body motions and the measurement of the inertial target line-of-sight angle rate. The tools for this work are the linear quadratic stochastic Gaussian optimal control theory coupled with the use of random-input describing functions. Although the use of the random-input describing function introduces an approximation in the work, it has been shown in the past that the use of random-input describing functions in miss distance calculations results in good approximations for the predicted miss distance. The paper includes the derivation of the optimal guidance law that accounts for both the missile acceleration limit and the constraint on the guidance gain and a simple one-dimensional Monte Carlo simulation to examine the performance of the guidance law.

I. Introduction

THE purpose of this paper is to derive and study a guidance law tailored to a missile with an acceleration bound and a limit on the allowable guidance gain. The limit on the guidance gain is a necessity imposed by the departure of the missile-to-target line-of-sight angular rate measurement mechanism from the ideal. In an ideal missile seeker, the measured inertial angular rate of the line of sight to the target is completely unaffected by the missile body's kinematics. This is rarely the case for practical missiles. The most well-known departure from this ideal situation is due to the variation of the radome slope (see Zarchan [1]). There are, however, other possible causes as well; these include seeker-head gyro sensitivity to acceleration, friction in the seeker bearings, finite stiffness of the wires connecting the imaging device in the seeker to the missile's body, gyro misalignment, etc. Any contamination of the measured target line-of-sight angular rate by the missile body's motions effectively limits the usable values of the navigation gain. If the navigation gain is too high for the given level of contamination, the missile oscillates at the characteristic autopilot frequency, resulting in large miss distances. This phenomenon has been most carefully studied for the case of varying radome slope, but as mentioned earlier, a similar effect is present in all practical missiles [1]. The purpose of this paper is to derive an optimal guidance law that takes into account both the bound on the missile's acceleration and the limit on the usable value of the navigation gain.

A simple approach to deriving a guidance law for a missile with a bound on its acceleration was presented in Rusnak [2] in a deterministic setting. A different approach to the guidance of missiles, with bounded acceleration in a nonstochastic setting, may be found in Gutman [3]. A stochastic optimal guidance law for a missile with bounded acceleration was derived in Hexner and Shima [4], and a linear approximation was derived in Hexner et al. [5]. The new guidance law was termed the saturated optimal guidance law (SOGL). The conclusions of these latter two papers were as follows:

1) The general form of the optimal guidance law [namely, that the interceptor acceleration command is proportional to the zero effort miss (ZEM)] is retained.

2) The bound on the missile acceleration renders the system nonlinear, so that the certainty equivalence principle is invalid.

3) The navigation gain depends upon both the magnitude of the observation noise and the interceptor maneuverability advantage over that of the target.

4) The optimal navigation gain reaches its peak value at a finite time before the target intercept.

5) The peak value of the navigation gain may reach extremely large values, sometimes exceeding 100. The large navigation gain in item 5 is shared with the linear quadratic optimal guidance law, where the navigation gain tends to infinity near the terminal time. In the guidance laws proposed in Hexner and Shima [4] and Hexner et al. [5], the missile acceleration reaches saturation earlier, generally resulting in better performance against maneuvering targets.

Would implementation of these guidance laws in a real missile lead to a retention of their desired performance? That depends on the size of the deviations of the target line-of-sight angular rate measurement from the ideal. As explained previously, some portion of the missile body angular rate contaminates the target line-of-sight angular rate measurement in most practical missiles. A sufficient condition for preventing missile instability, and the resulting increase in miss distance, is to impose a limit on the maximum allowed value of the navigation gain. This undoubtedly carries with it a loss of performance, but it is necessary if the guidance algorithm is to be implemented in a practical missile. This is not very different from good practice in control design, where some performance is sacrificed for the sake of reliability and robustness.

The main approximation used in the paper to arrive at a tractable optimization problem is the use of the random-input describing function (RIDF), found in Gelb and Vander Velde [6]. The use of this method for estimating the miss distance in missiles was employed in a paper by Zarchan [7], where the statistics of the miss distances predicted by the use of the RIDF approximation were shown to lead to reasonable agreement with the miss distance statistics obtained by

Presented as Paper 2010-8054 at the AIAA GNC 2010 Conference, Toronto, Ontario, Canada, 8 February–8 May 2010; received 10 July 2010; revision received 29 October 2010; accepted for publication 29 October 2010.

*Research Associate.
†Simulation Engineer, Central Laboratory Division.

nonlinear simulation. The statistical description of the target maneuver in [7] was based upon the use of shaping filters, described by Singer [8] and Fitzgerald [9].

The idea of using the RIDF approximation to solve an optimal regulator problem was introduced by Gokcek et al. [10]. These ideas were further extended to the time varying case by Hexner et al. [5] and are also used in this paper.

The novelty of the paper is the derivation of an optimal guidance law for a bounded acceleration missile subject to a limit on the guidance gain. The new guidance law is denoted as the limited SOGL (LSOGL).

The problem formulation is presented in Sec. II, and the necessary conditions for the optimal guidance gain are derived in Sec. III. This is followed by Sec. IV, which presents the graphs of the optimal guidance gains for a range of the problem parameters and the miss distances obtained from a Monte Carlo simulation using the new LSOGL guidance law.

II. Problem Formulation

The problem studied here is the terminal guidance of an interceptor missile. It is assumed that the interceptor and its target are both near the collision course. In this case, the dynamics of the final miss are well represented by analyzing the equations of motion perpendicular to the initial line of sight.

A. Equations of Motion

The equations of motion used here describe the dynamics perpendicular to the initial line-of-sight direction. The main variables are the relative position and velocity of the interceptor and the target (p and v, respectively) as well as the interceptor and the target accelerations, denoted as a_M and a_T, respectively; all are perpendicular to the initial line-of-sight direction. The target acceleration a_T is modeled as a first-order Gauss–Markov random process:

$$\dot{a}_T = -\frac{1}{\tau_T} a_T + w \tag{1}$$

where w is a white noise process with spectral density W. The missile acceleration response to an acceleration command a_c is

$$\dot{a}_M = -\frac{1}{\tau_M} a_M + \frac{1}{\tau_M} \text{sat}(a_c) \tag{2}$$

where

$$\text{sat}(a_c) = \begin{cases} A_c & a_c > A_c \\ a_c & -A_c \le a_c \le A_c \\ -A_c & a_c < -A_c \end{cases} \tag{3}$$

and where A_c is the bound on the missile acceleration.

Defining the state vector $\boldsymbol{x}$,

$$\boldsymbol{x} = [\, p \quad v \quad a_M \quad a_T \,]' \tag{4}$$

the equations of motion may be expressed compactly as

$$\dot{\boldsymbol{x}} = \boldsymbol{A}\boldsymbol{x} + \boldsymbol{B}\text{sat}(a_c) + \boldsymbol{G}w \tag{5}$$

where

$$\boldsymbol{A} = \begin{bmatrix} 0 & 1 & 0 & 0 \\ 0 & 0 & -1 & 1 \\ 0 & 0 & -1/\tau_M & 0 \\ 0 & 0 & 0 & -1/\tau_T \end{bmatrix} \tag{6}$$

$$\boldsymbol{B} = \begin{bmatrix} 0 \\ 0 \\ 1/\tau_M \\ 0 \end{bmatrix} \tag{7}$$

$$\boldsymbol{G} = \begin{bmatrix} 0 \\ 0 \\ 0 \\ 1 \end{bmatrix} \tag{8}$$

B. Criterion

The optimal guidance law that is sought minimizes the cost function J:

$$J = \boldsymbol{E}\left\{ \boldsymbol{x}'(T_f)\boldsymbol{Q}_f\boldsymbol{x}(T_f) + \int_0^{T_f} a_c^2(t)\,\mathrm{d}t \right\} \tag{9}$$

subject to Eq. (5) and the navigation gain magnitude constraint. The terminal weighting matrix $\boldsymbol{Q}_f$ is

$$\boldsymbol{Q}_f = \begin{bmatrix} q_f & 0 & 0 & 0 \\ 0 & 0 & 0 & 0 \\ 0 & 0 & 0 & 0 \\ 0 & 0 & 0 & 0 \end{bmatrix} \tag{10}$$

C. Measurements

The missile observes the inertial line-of-sight angle λ between the initial line-of-sight direction and the current angular position of the target, with the addition of white additive noise n with spectral density equal to R:

$$y = \lambda + n \tag{11}$$

and λ is approximated as

$$\lambda = p/r \tag{12}$$

where r is the projection of the range between the interceptor and the target onto the initial inertial line-of-sight direction. It is assumed that the range between the target and the intercepting missile is known with negligible error, so that the only randomness introduced by the measurements is in the observation of the angle λ in Eq. (11). In matrix–vector notation, the observation is expressed as

$$y = \boldsymbol{C}\boldsymbol{x} + n \tag{13}$$

where

$$\boldsymbol{C} = [\, 1/r \quad 0 \quad 0 \quad 0 \,] \tag{14}$$

III. Problem Solution

The solution is obtained in two steps. First, the system dynamics are expressed in terms of the ZEM. Second, the cost function is expressed in terms of the conditional expectation of the ZEM.

A. Transformation to Zero Effort Miss

The use of the ZEM Z reduces the number of state variables from four to one. The ZEM is defined as

$$Z = p + vt_g + a_T\tau_T^2\psi(t_g/\tau_T) - a_M\tau_M^2\psi(t_g/\tau_M) \tag{15}$$

where t_g is the time until the intercept, $t_g = T_f - t$, and ψ is

$$\psi(\zeta) = e^{-\zeta} + \zeta - 1 \tag{16}$$

By straightforward differentiation, it is found that

$$\dot{Z} = -\text{sat}(a_c)\tau_M\psi(t_g/\tau_M) + \tau_T^2\psi(t_g/\tau_T)w \tag{17}$$

and since at $t = T_f$, $t_g = 0$, $\psi(\zeta) = 0$, and $Z(T_f) = p(T_f)$, the criterion function may be simplified to

$$J = \boldsymbol{E}\left\{ q_f Z^2(T_f) + \int_0^{T_f} a_c^2(t)\,\mathrm{d}t \right\} \tag{18}$$

Note that this reduction to a single state variable Z does not involve any approximations and is valid as long as the only nonlinearity in the system is the acceleration saturation.

The conditional expectation $\hat{Z} = \boldsymbol{E}\{Z|y(s)s < t\}$ may be calculated using the ubiquitous Kalman filter. The state vector for the Kalman filter is $\boldsymbol{z}$:

$$\boldsymbol{z} = [\,Z \quad v \quad a_M \quad a_T\,]' \tag{19}$$

and the process model for the Kalman filter is

$$\dot{\boldsymbol{z}} = \boldsymbol{A}_z \boldsymbol{z} + \boldsymbol{B}_z \,\mathrm{sat}(a_c) + \boldsymbol{G}_z w \tag{20}$$

where

$$\boldsymbol{A}_z = \begin{bmatrix} 0 & 0 & 0 & 0 \\ 0 & 0 & -1 & 1 \\ 0 & 0 & -1/\tau_M & 0 \\ 0 & 0 & 0 & -1/\tau_T \end{bmatrix} \tag{21}$$

$$\boldsymbol{B}_z = [\,-\tau_M \psi(t_g/\tau_M) \quad 0 \quad 1/\tau_M \quad 0\,]' \tag{22}$$

$$\boldsymbol{G}_z = [\,\tau_T^2 \psi(t_g/\tau_T) \quad 0 \quad 0 \quad 1\,]' \tag{23}$$

The observations are now expressed as

$$y = \boldsymbol{C}_z \boldsymbol{z} + n \tag{24}$$

where

$$\boldsymbol{C}_z = [\,1 \quad -t_g \quad \tau_M^2 \psi(t_g/\tau_M) \quad -\tau_T^2 \psi(t_g/\tau_T)\,]/r \tag{25}$$

B. Kalman Filter

The Kalman filter is independent of both the missile acceleration bound and the limit on the guidance gain. The form of the Kalman filter for calculating the conditional expectation $\hat{\boldsymbol{z}} = \boldsymbol{E}\{\boldsymbol{z}|y(s)s < t\}$ is

$$\dot{\hat{\boldsymbol{z}}} = \boldsymbol{A}_z \hat{\boldsymbol{z}} + \boldsymbol{B}_z \,\mathrm{sat}(a_c) + \boldsymbol{K}_f \eta \tag{26}$$

where

$$\eta = y - \boldsymbol{C}_z \hat{\boldsymbol{z}} \tag{27}$$

is the innovations process for which the autocovariance is

$$\mathbf{E}\,\{\eta(t)\eta(t+s)\} = \delta(s)\sigma_\eta^2 = \delta(s)R \tag{28}$$

or

$$\sigma_\eta = \sqrt{(R)} \tag{29}$$

and where $\boldsymbol{K}_f$ is the Kalman filter gain:

$$\boldsymbol{K}_f = \boldsymbol{P}\boldsymbol{C}_z' R^{-1} \tag{30}$$

The covariance matrix of the error in the estimate $\boldsymbol{P}$ is obtained by solving the Riccati differential equation,

$$\dot{\boldsymbol{P}} = \boldsymbol{A}_z \boldsymbol{P} + \boldsymbol{P}\boldsymbol{A}_z' - \boldsymbol{P}\boldsymbol{C}_z' R^{-1} \boldsymbol{C}_z \boldsymbol{P} + \boldsymbol{G}_z W \boldsymbol{G}_z' \tag{31}$$

The initial condition for solving [Eq. (31)] $\boldsymbol{P}(0)$ is the covariance matrix for the state vector [Eq. (19)] at the initial time.

C. Reduction to First Order

Let $\tilde{Z} = \hat{Z} - Z$ be the estimator error. Note that the saturation nonlinearity enters the Kalman filter only through the deterministic input, so that the Kalman filter is a true calculation of the conditional expectation, $\boldsymbol{E}\{Z|y(s)s < t\}$. Therefore, the estimation error $\tilde{Z}$ and the estimate $\hat{Z}$ are independent. Then, the criterion function may be further rewritten as

$$J = J_Z + J_e \tag{32}$$

where

$$J_Z = \boldsymbol{E}\left\{\hat{Z}^2(T_f) q_f + \int_0^{T_f} a_c^2(t)\,\mathrm{d}t\right\} \tag{33}$$

$$J_e = \boldsymbol{E}\{\tilde{Z}^2(T_f)\} q_f \tag{34}$$

and $\hat{Z}$ obeys the stochastic differential equation:

$$\dot{\hat{Z}} = -\tau_M \psi(t_g/\tau_M)\mathrm{sat}(a_c) + (\boldsymbol{K}_f)_1 \eta \tag{35}$$

where $(\boldsymbol{K}_f)_1$ is the first component of the Kalman gain defined in Eq. (30). The expression J_e in Eq. (34) is unaffected by the choice of a_c. The main problem has been reduced to minimizing J_Z in Eq. (33) subject to Eq. (35). Then, the conclusion is that the conditional expectation $\hat{Z} = \boldsymbol{E}\{Z|y(s)s < t\}$ is a sufficient statistic for minimizing Eq. (33) and that the optimal missile acceleration command is a function of $\hat{Z}$ only.

D. Two Approximations

Two approximations are required to reduce the problem to tractable form. In principle, the optimization problem posed in Eqs. (33) and (35) may have a nonlinear solution. The first approximation is to restrict the possible minimizers to the form of a linear, but time-varying, function of $\hat{Z}$. That is, only functions of the form

$$a_c = \left(\frac{N'\hat{Z}}{t_g^2}\right) \tag{36}$$

are considered. In Eq. (36), N' may be recognized as the navigation gain, which is bounded:

$$N' \le N'_{\max} \tag{37}$$

The second approximation is to use the RIDF to approximate the saturation function when Eq. (36) is substituted into Eq. (35). Performing the substitution and using the RIDF approximation,

$$\dot{\hat{Z}} \approx -\tau_M \psi(t_g/\tau_M) L \frac{N'\hat{Z}}{t_g^2} + (\boldsymbol{K}_f)_1 \eta \tag{38}$$

where L is the RIDF corresponding to the sat function in Eq. (36). The RIDF approximation is presented in the Appendix [see Eq. (A1) for the definition].

E. Derivation of Necessary Conditions

The derivation is carried out in two steps:

1) The expectation in Eq. (33) is evaluated.

2) The necessary conditions are derived for the evaluated expressions.

Using our assumption [Eq. (36)] the expression for J_Z in Eq. (33) is evaluated as

$$\begin{aligned} J_Z &= \boldsymbol{E}\left\{\hat{Z}^2(T_f) q_f + \int_0^{T_f} a_c^2(t)\,\mathrm{d}t\right\} \\ &= P_{\hat{Z}\hat{Z}}(T_f) q_f + \int_0^{T_f} \left(\frac{N'(t_g)}{t_g^2}\right)^2 P_{\hat{Z}\hat{Z}}\,\mathrm{d}t \end{aligned} \tag{39}$$

where

$$P_{\hat{Z}\hat{Z}} = \boldsymbol{E}\{\hat{Z}\,\hat{Z}\} \tag{40}$$

The covariance matrix $P_{\hat{Z}\hat{Z}}$ evolves according to the Lyapunov equation:

$$\dot{P}_{\hat{z}\hat{z}} = -\frac{2\tau_m \psi(t_g/\tau_m)}{t_g^2} LN' P_{\hat{z}\hat{z}} + (\boldsymbol{K}_f)_1^2 \sigma_\eta^2 \tag{41}$$

for which the initial condition is simply the covariance of the conditional expectation of the ZEM Z at the initial time. The problem has been transformed to minimizing Eq. (39) subject to Eq. (41), and

$$L = \operatorname{erf}\left(\frac{A_c}{\sqrt{2}\sigma_{a_c}}\right) = \operatorname{erf}\left(\frac{A_c t_g^2}{N'\sqrt{2P_{\hat{z}\hat{z}}}}\right) \tag{42}$$

Following Gokcek et al. [10], the Hamiltonian associated with the problem is

$$H = \left(\frac{N'}{t_g^2}\right)^2 P_{\hat{z}\hat{z}} + S\left[-\frac{2\tau_m \psi(t_g/\tau_m)}{t_g^2} LN' P_{\hat{z}\hat{z}} + (\boldsymbol{K}_f)_1^2 \sigma_\eta^2\right] + \xi\left[\left(\frac{N'}{t_g^2}\right)^2 P_{\hat{z}\hat{z}} - \frac{A_c^2}{2[\operatorname{erf}^{-1}(L)]^2}\right] \tag{43}$$

where S and ξ are Lagrange multipliers. The optimization variables are N' and L [subject to the constraint equation (42)]. Their optimal values, $(N')^*$ and L^*, satisfy (see Bryson and Ho [11])

$$(N')^*, \qquad L^* = \arg\min_{N',L} H \tag{44}$$

subject to $N' \le N'_{\max}$,

$$\dot{S} = -\frac{\partial H}{\partial P_{\hat{z}\hat{z}}} \tag{45}$$

and the transversality condition:

$$S(T_f) = q_f \tag{46}$$

The necessary conditions are derived separately for the case when N' is less than its allowed maximum value, $N'_{\max}$ and then for the case when the constraint equation (37) is active. Subsequently, a complete algorithm is presented covering both cases.

1. N' not Saturated

When the constraint equation (37) is not active, the development is similar to that presented in Hexner et al. [5]. Since the Hamiltonian equation (43) is quadratic in N', it may be minimized by setting the derivative of H, with respect to N', to zero and solving the resulting equation, which is

$$N' = \frac{\tau_M \psi(t_g/\tau_M) LS t_g^2}{1+\xi} \tag{47}$$

Performing the differentiation indicated in Eq. (45) and substituting Eq. (47) yields the differential equation for the adjoint variable S:

$$\dot{S} = \frac{\tau_M^2 \psi^2(t_g/\tau_M) L^2 S^2}{1+\xi} \tag{48}$$

The terminal condition for this differential equation is given by Eq. (46). Taking the derivative of H with respect to L yields

$$\frac{\partial H}{\partial L} = -2\tau_M \psi(t_g/\tau_M)\frac{N'}{t_g^2} P_{\hat{z}\hat{z}} S - \xi \frac{A_c^2}{2}(-2)[\operatorname{erf}^{-1}(L)]^{-3}\frac{\operatorname{derf}^{-1}(L)}{\mathrm{d}L} \tag{49}$$

Using

$$\left(\frac{N'}{t_g^2}\right)^2 P_{\hat{z}\hat{z}} = \frac{A_c^2}{2[\operatorname{erf}^{-1}(L)]^2} \tag{50}$$

and Eqs. (47) and (A6) in Eq. (49),

$$\frac{\partial H}{\partial L} = \frac{-2\tau_M^2 \psi^2(t_g/\tau_M) P_{\hat{z}\hat{z}} LS^2}{1+\xi} + \xi\left(\frac{N'}{t_g^2}\right)^2 P_{\hat{z}\hat{z}}\sqrt{\pi}\frac{\exp\{[\operatorname{erf}^{-1}(L)]^2\}}{\operatorname{erf}^{-1}(L)} \tag{51}$$

Using the optimal value of N' [Eq. (47) in Eq. (51)], setting $\frac{\partial H}{\partial L}$ equal to zero, and simplifying,

$$\xi = \frac{2}{L\sqrt{\pi}[(\exp\{[\operatorname{erf}^{-1}(L)]^2\})/\operatorname{erf}^{-1}(L)] - 2} \tag{52}$$

Taking the positive square root of Eq. (50) and substituting the expression for the optimal value of N' [Eq. (47)],

$$\tau_M \psi(t_g/\tau_M)\sqrt{P_{\hat{z}\hat{z}}} S = \frac{1+\xi}{L}\frac{A_c}{\sqrt{2}\operatorname{erf}^{-1}(L)} \tag{53}$$

Substituting Eq. (52) into Eq. (53) results in a single equation in L:

$$\frac{\tau_M \psi(t_g/\tau_M)\sqrt{P_{\hat{z}\hat{z}}} S}{A_c} = \frac{1 + (2/\{\sqrt{\pi}L[(\exp\{[\operatorname{erf}^{-1}(L)]^2\})/\operatorname{erf}^{-1}(L)] - 2\}}{L}\frac{1}{\sqrt{2}\operatorname{erf}^{-1}(L)} \tag{54}$$

2. N' Constraint is Active

When the constraint on the navigation constant is active, the value of the RIDF L is obtained from Eq. (42):

$$L = \operatorname{erf}\left\{\frac{A_c t_g^2}{\sqrt{2}N'_{\max}\sqrt{P_{\hat{z}\hat{z}}}}\right\} \tag{55}$$

The Hamiltonian is minimized with respect to L by setting its derivative with respect to L equal to zero. The derivative is the same as in Eq. (49) but with N' replaced by $N'_{\max}$. Using the inverse form of Eq. (55),

$$\left(\frac{N'}{t_g^2}\right)^2 P_{\hat{z}\hat{z}} = \frac{A_c^2}{2[\operatorname{erf}^{-1}(L)]^2} \tag{56}$$

and the calculation of the derivative from the Appendix [Eq. (A6)],

$$\xi = \frac{2\tau_M \psi(t_g/\tau_M) S}{(N'_{\max}/t_g^2)\sqrt{\pi}[(\exp\{[\operatorname{erf}^{-1}(L)]^2\})/\operatorname{erf}^{-1}(L)]} \tag{57}$$

The differential equation for S is obtained by carrying out the differentiation indicated in Eq. (45):

$$\dot{S} = -(\xi+1)\left(\frac{N'_{\max}}{t_g^2}\right)^2 + 2\tau_M \psi(t_g/\tau_M) L\frac{N'_{\max}}{t_g^2} S \tag{58}$$

3. Solution Method

The algorithm used to solve the two-point boundary value problem is essentially a first-order differential dynamic program (Jacobson and Mayne [12]). In practice, the algorithm converges after about 5–10 iterations. The solution steps are outlined in Table 1, and the acceleration command implemented and tested in this paper is of the following form:

$$a_c = \left(\frac{N'\hat{Z}}{t_g^2}\right) \tag{59}$$

There is no proof of convergence of this algorithm. However, in [10], a proof is provided for the convergence of a similar algorithm connected with the linear quadratic regulator problem with bounded input.

Table 1 Calculation of N'

Step	Description
	Preliminary calculations
1	Solve the Kalman filter equations (30) and (31) and store $\boldsymbol{K}_f$ and σ_η.
2	Assume initial values $N' = 3$, $L = 1$, and $\xi = 0$.
	Iteration
3	Solve the differential equation (41) and store $P_{\hat{Z}\hat{Z}}$.
4	Calculate S.
	At each integration step, solve Eq. (54) for L and substitute into Eq. (52).
	If $N' < N'_{\max}$, use Eq. (48) for the integration step; otherwise, solve Eqs. (55) and (57) and use Eq. (58) for the integration step.
5	If the change in N' is sufficiently small, exit; otherwise, go to step 3.

IV. Numerical Calculations and Simulation Results

The calculations were carried out for a range of parameter values. The measurements [Eq. (11)] were assumed to be taken every T_s s, and the standard deviation of the measurement noise for each measurement was σ_e. The additive observation noise standard deviation σ_e varied as a function of the range between the missile and the target:

$$\begin{aligned} \sigma_e &= \sigma_n, \qquad r > r_c \\ &= \sigma_n \frac{r}{r_c}, \qquad r < r_c \end{aligned} \tag{60}$$

The variation of σ_e is a very simplified model for glint. For the development of the necessary optimality conditions, a continuous time measurement model was assumed. In the continuous model, the noise intensity was characterized by its power spectral density R. The equivalent intensity of the continuous time noise was calculated as

$$R = T_s \sigma_e^2 \tag{61}$$

Some of the results of the calculation of the optimal navigation gain are presented in Figs. 1–3. The values of the basic parameters are shown in Table 2.

Figure 1 presents the variation of the navigation gain as the intercepting missile's maximum acceleration capability takes on the values of 100, 150, 250, and ∞, while there is no bound on the navigation gain N'. The legend in of the figure represents the interceptor acceleration limit. Note that, for the unbounded missile acceleration case, the navigation gain of the linear quadratic Gaussian optimal guidance law is recovered. It is seen that the navigation gain is very much influenced by the acceleration capability of the missile. The target observation noise was 1 mrad. In particular, two trends (already noted in Hexner et al. [5]) may be observed. First, the peak of the navigation gain occurs earlier on in the engagement scenario for the missile with bounded acceleration as compared with the unbounded one. Second, the navigation gain is significantly larger earlier on for the bounded as compared with the unbounded acceleration case. When no bound is assumed on the missile's acceleration capability, the guidance law postpones closing the miss distance to as late as possible in order to benefit from the additional target observations available for calculating the commanded missile acceleration close to the terminal time. When the missile acceleration is bounded, such a policy is not efficient, since the missile's limited acceleration capability may not enable it to close the miss distance. For the largest values of the navigation gain

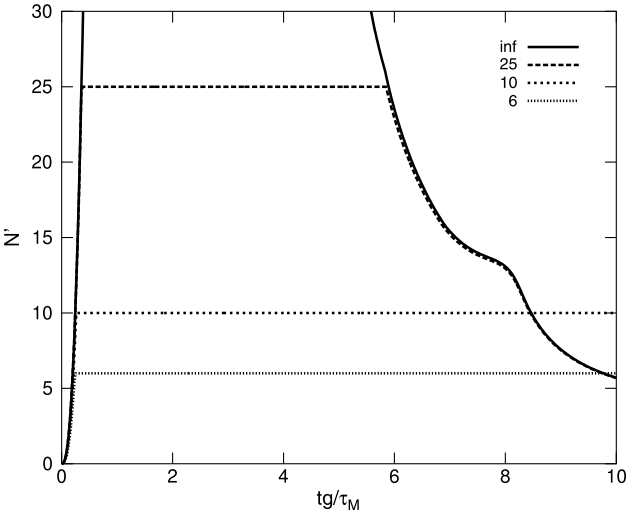

Fig. 2 The variation N' with $N'_{\max}$: $Ac = 150$ m/s^2 and $\sigma_e = 1.0$ mrad.

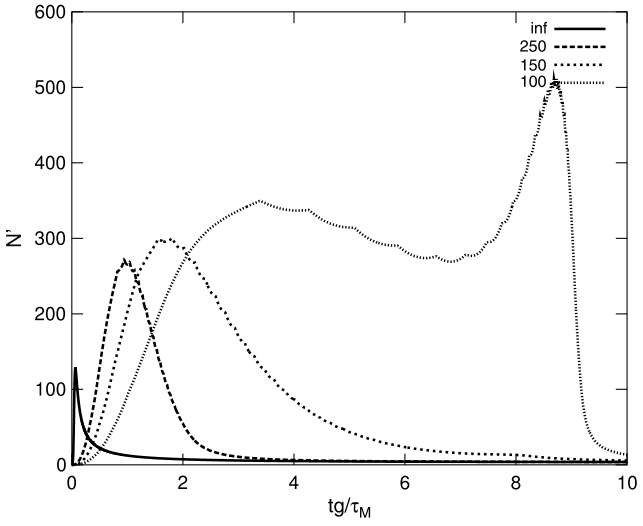

Fig. 1 The variation N' with missile acceleration limit: $\sigma_e = 1.0$ mrad.

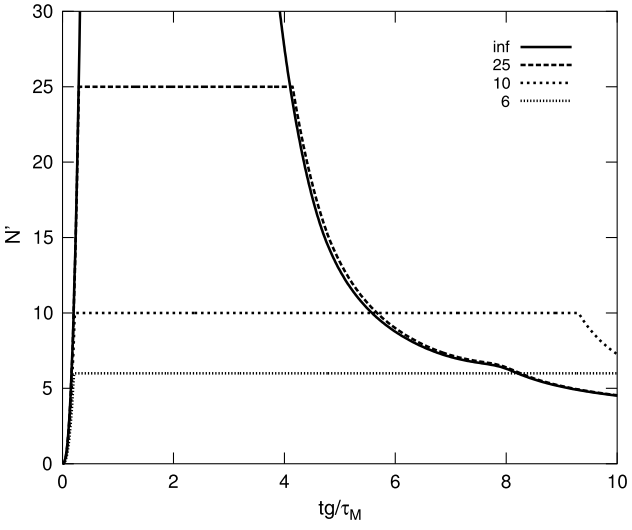

Fig. 3 The variation N' with $N'_{\max}$: $Ac = 150$ m/s^2 and $\sigma_e = 0.5$ mrad.

Table 2 Parameter values used in the calculations

Symbol	Value	Description
τ_M, s	0.2	Missile time constant
τ_T, s	3.0	Target acceleration decorrelation time
V_c, m/s	1000	Closing velocity
r_c, m	100	Range where glint becomes significant
σ_a, m/s^2	50	Target acceleration standard deviation
q_f, 1/m^2	10^{10}	Terminal weight on the miss distance
T_s, s	0.01	Target measurement interval
σ_n, mrad	0.2–1.0	Additive target measurement noise
σ_Z, m	5	Standard deviation of ZEM at the initial time
σ_v, m/s	5	Standard deviation of v at the initial time
σ_{aT}, m/s^2	5	Standard deviation of a_T at the initial time

appearing in Fig. 1, the guidance law is essentially equivalent to the bang–bang law, $a_c = A_c \operatorname{sign}(Z)$.

Figure 2 depicts the influence of the maximum value of the guidance gain $N'_{\max}$ on the time variation of N'. Curves are shown for values of 6, 10, 25, and unbounded $N'_{\max}$ for the same value of the standard deviation of the observation noise, $\sigma_e = 1$ mrad (as in Fig. 1). The legend represents the limit imposed on the navigation gain. When the bound on the guidance gain $N'_{\max}$ is equal to 25, or larger, then, for the time instants when the bound is not active, the values obtained for N' nearly coincide with the values obtained for the unbounded case. However, when $N'_{\max}$ is equal to 6 or 10, the guidance gain is significantly larger than in the unbounded case for a normalized time to go, t_g/τ_M, greater than about 9.3. The standard deviation of the target observation noise was 1 mrad.

Figures 3 and 4 present the same variation as Fig. 2, but now the standard deviation of the observation noise σ_n is equal to 0.5 and 0.1 mrad, respectively. Again, the legend represents the limit on the navigation gain. The influence of decreasing the observation noise may be observed by comparing Fig. 2 on the one hand and Figs. 3 and 4 on the other hand. It is seen that, qualitatively, the figures are similar, but now the larger values of the navigation gain appear closer to the intercept time than in Fig. 2, a trend observed in Hexner et al. [5]. It is seen that, when $N'_{\max} = 25$ (and for larger values), the guidance gain is, again, simply a limited version of the unbounded guidance gain. In contrast, for smaller values of $N'_{\max}$, the guidance gain takes on larger gain values than the values taken on by the guidance gain when it is unbounded. The assumed missile acceleration limit in Figs. 2–4 was 150 m/s^2.

To examine the impact on the miss distance, a one-dimensional Monte Carlo simulation was run. The simulation modeled a target with a 0.3 s time constant being intercepted. Each Monte Carlo set consisted of 1000 runs. The simulations were set up to have each set use the same seed so that the random variables for all run sets would have the same values.

The simulation was run using two distinct target maneuver command models, but in each case, the target acceleration commands were passed through a first-order lag with a time constant of 0.3 s, which modeled the target's assumed time constant. The first set of simulations was carried out by directly simulating the acceleration commands according to Eq. (1); for the second set, the target maneuver model consisted of a single commanded acceleration step. The time of the step was distributed uniformly throughout the simulation interval, and the amplitude of the step was drawn from a Gaussian distribution. The standard deviation of the target acceleration was identical for the two target maneuver command models. The results for the first target maneuver model are presented in Figs. 5–8, and for the second model, the results appear in Figs. 9–12. The values used in the simulations are listed in Table 2. Note that, in neither simulation set does the assumed target maneuver model match what was actually employed in the simulations, and the miss match is most pronounced for the second target acceleration command model. For the first simulation set, there is an extra first-order lag with a time constant of 0.3 s, not accounted for in Eq. (1). In the second set, the target maneuver is a single acceleration step, with the onset of the maneuver uniformly distributed.

The parasitic coupling in the missile body motions into the estimated line-of-sight rate is not modeled in the simulations. Instead, it was assumed that the limit on the guidance gain is such that the influence of these parasitic coupling effects was negligible.

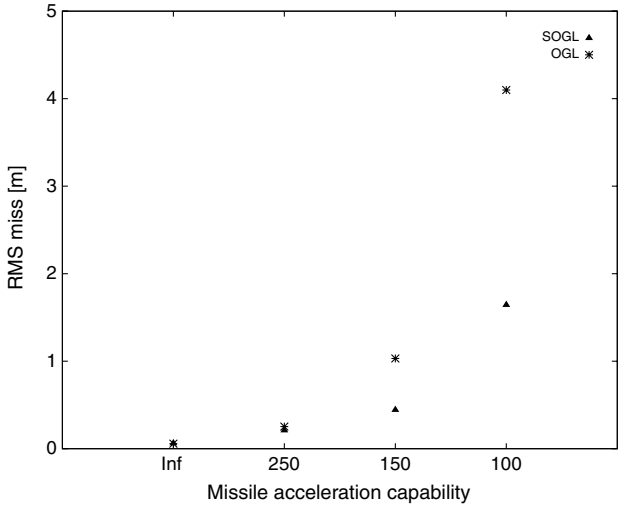

Fig. 5 RMS miss distances for bounded missile acceleration and unbounded guidance gain $N'_{\max}$: first target acceleration model.

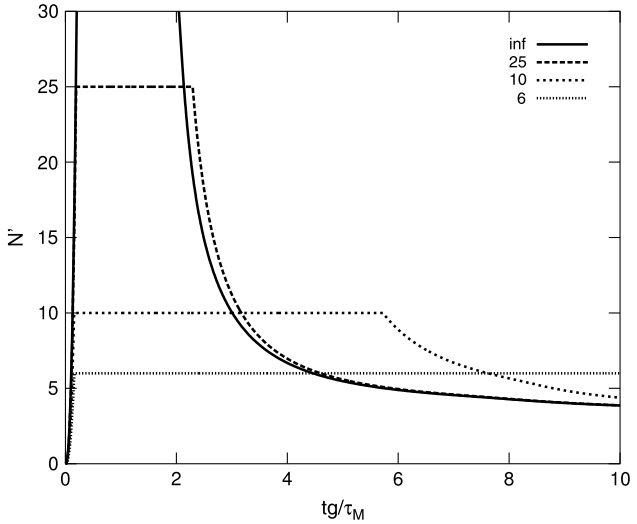

Fig. 4 The variation N' with $N'_{\max}$: $Ac = 150$ m/s^2 and $\sigma_e = 0.1$ mrad.

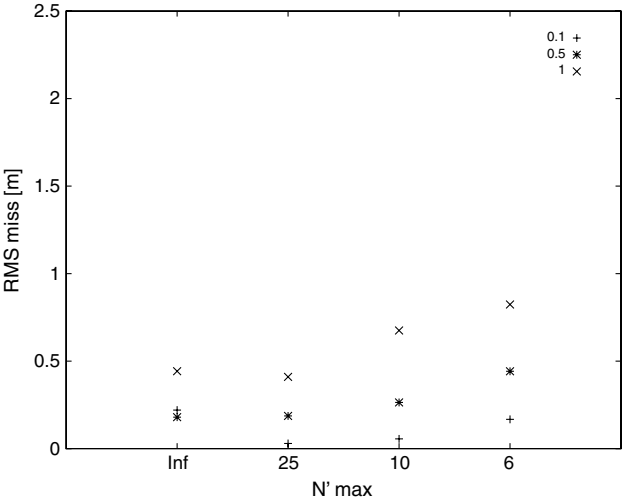

Fig. 6 RMS miss distances for varying $N'_{\max}$: first target acceleration model.

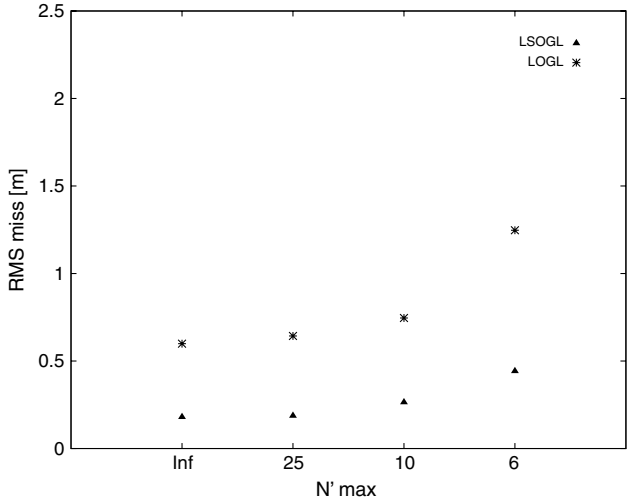

Fig. 7 Comparison of rms miss distances $\sigma_n = 0.5$ mrad: first target acceleration model.

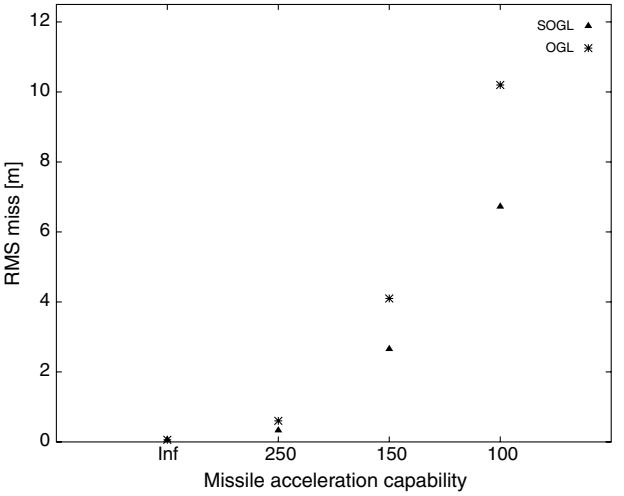

Fig. 9 RMS miss distances for bounded missile acceleration and unbounded guidance gain $N'_{\max}$: second target acceleration model.

In Fig. 5, the rms miss distances are shown as a function of the missile's acceleration limit when there is no limit on N'. The * symbol denotes the rms miss distances obtained when the linear Gaussian optimal guidance law gain is used. The triangles represent the rms miss distances obtained when the gain (SOGL) is calculated according to the algorithm in Sec. III.E.3 and the missile's acceleration limit matches that assumed by the gain calculation algorithm, but there is no limit on the allowed values of the guidance gain N'. It is seen that the use of the matched guidance gain values significantly reduces the miss distance. Figure 6 depicts the influence of the value of $N'_{\max}$, the bound on N', on the resulting rms miss distances for three values of the standard deviation of the additive observation noise: 0.1, 0.5, and 1 mrad, as indicated by the legend of the figure. First, it is observed that decreasing $N'_{\max}$ changes the miss distance by a small value when going from an unbounded N' down to 10. On the other hand, the change from 10 to 6 causes a definite increase in the miss distance. This increase in rms miss distance is the price paid for making the guidance system robust to parasitic coupling between the body dynamics and the estimation of the inertial line-of-sight angular rate measurement mechanism. The results indicate that this effect increases with increasing measurement noise.

Next, the rms miss distances obtained from the guidance gain calculation of Sec. III are compared with the miss distances resulting from the use of the linear quadratic Gaussian optimal guidance gain values limited to the appropriate $N'_{\max}$. Figures 7 and 8 show the miss distances when the additive observation noise is 0.5 and 1 mrad, respectively. The abscissa shows $N'_{\max}$, the limit on the guidance gain, and the ordinate shows the resulting rms miss distances. The * represents the rms miss distances obtained when the linear quadratic Gaussian optimal guidance gain is limited to the values indicated on the horizontal axis, and the triangles represent the rms miss distances obtained from the use of the guidance gain calculated by the algorithm in Sec. III (LSOGL). In both figures, the missile acceleration limit was 150 $\mathrm{m/s^2}$. It is seen that the use of the guidance gain values LSOGL, calculated according to Sec. III, result in significantly lower miss distances than simply limiting the gain values of the optimal guidance law.

The simulation results derived from simulating the second target acceleration model are now presented. In Fig. 9, the rms miss distances derived from the use of the optimal guidance law and from SOGL guidance laws are compared for the second target acceleration command model. Again, as in Fig. 5, the use of the SOGL guidance, as derived in Sec. III.E.3, significantly reduces the miss distance. Note the differing vertical scales used in Figs. 5 and 9. The differing vertical scales reflect the more difficult maneuver of the second target acceleration command. The influence of the value of $N'_{\max}$, the bound on the guidance gain N', on the rms miss distances is presented for three values of the observation noise: 0.1, 0.5 and 1 mrad, as indicated by the legend in Fig. 10. The rms miss distances obtained from the guidance gain calculation of Sec. III are compared with the miss distances resulting from the use of the linear quadratic Gaussian

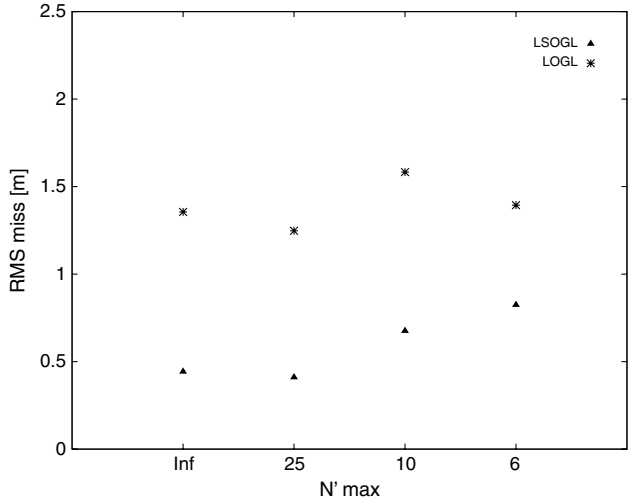

Fig. 8 Comparison of rms miss distances $\sigma_n = 1$ mrad: first target acceleration model.

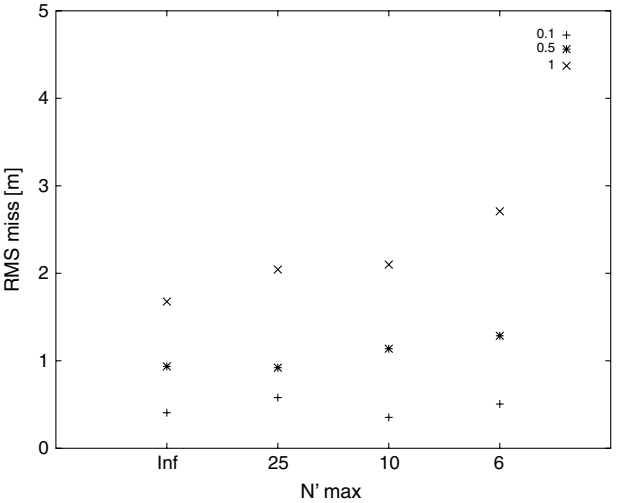

Fig. 10 RMS miss distances for varying $N'_{\max}$: second target acceleration model.

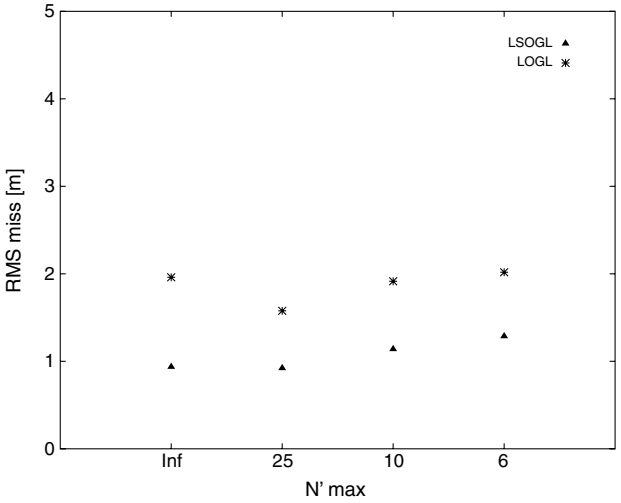

Fig. 11 Comparison of rms miss distances $\sigma_n = 0.5$ mrad: second target acceleration model.

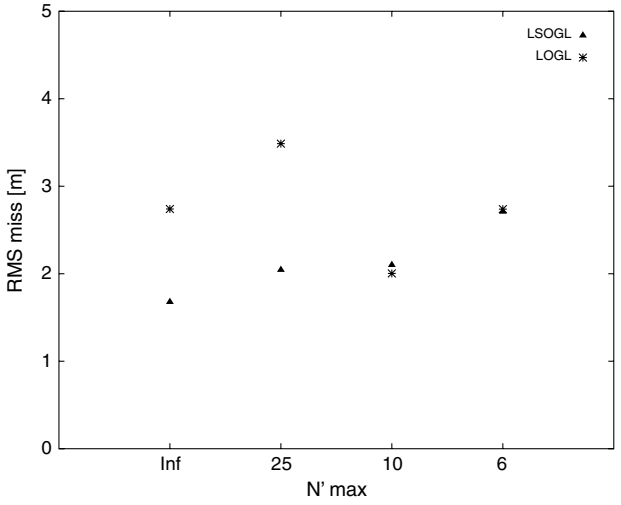

Fig. 12 Comparison of rms miss distances $\sigma_n = 1$ mrad: second target acceleration model.

optimal guidance gain values limited to the appropriate $N'_{\max}$ using the second target acceleration model. Figures 11 and 12 show the miss distances when the additive observation noise is 0.5 and 1 mrad, respectively. The abscissa shows $N'_{\max}$, the limit on the guidance gain, and the ordinate shows the resulting rms miss distances. The * represents the rms miss distances obtained when the linear quadratic Gaussian optimal guidance gain is limited to the values indicated on the horizontal axis, and the triangles represent the rms miss distances obtained from the use of the guidance gain calculated by the algorithm in Sec. III (LSOGL). In both figures, the missile acceleration limit was 150 m/s^2. It is seen that the use of the guidance gain values LSOGL, calculated according to Sec. III, result in significantly lower miss distances than simply limiting the gain values of the optimal guidance law; however, for the second target acceleration model, the results are less regular than for the first acceleration model. (Note the different values used for the vertical scales of the figures for the miss distances of the second target acceleration command model.)

V. Conclusions

In this paper, a stochastic optimal guidance law was derived, which takes into account the missile's acceleration bounds and limits the guidance gain N'. The limit on the guidance gain is necessitated by the departure of the missile's angular line-of-sight rate calculation from ideal, caused by various parasitic coupling mechanisms between the missile body's angular motions and the seeker. Ignoring this parasitic coupling in the design of the guidance law may cause instability in the missile body's motion and eventually increases the miss distance.

The bound on the missile's acceleration results in an increase in the guidance gain earlier in the scenario as compared with the guidance gain obtained from the linear quadratic Gaussian optimal guidance law. Similarly, placing explicit limits on the maximum usable guidance gain also has the effect of increasing the guidance gain earlier in the scenario. Both of these effects are influenced by the seeker target's angular measurement noise. Decreasing the measurement noise allows for the increase in the guidance gain to take place closer to the intercept point.

The new guidance law was incorporated into a simple one-dimensional guidance Monte Carlo simulation. The results of the Monte Carlo simulation show that decreasing values of the guidance gain bound somewhat increases (as expected) the rms miss distance; however, this is the price to be paid for the robustness of the guidance system when faced with possible parasitic coupling between the missile body angular motions and the mechanism for the measurement of the inertial target line-of-sight rate.

Appendix: Random-Input Describing Functions

RIDFs approximate nonlinearities in a stochastic setting and, in many cases, lead to useful approximate analysis of nonlinear problems. Let $\phi(\zeta)$ be an odd nonlinearity driven by a zero-mean Gaussian process. The nonlinearity $\phi(\zeta)$ is approximated by the linear $L\zeta$ by solving the following minimization problem:

$$\min_L \boldsymbol{E}\{[\phi(\zeta) - L\zeta]^2\} \tag{A1}$$

where L is called the RIDF. The L that minimizes Eq. (A1), for the saturation function $\phi(\zeta)$, as defined in Eq. (3), is achieved by Gelb and Vander Velde [6]:

$$L = \operatorname{erf}\left(\frac{A_c}{\sqrt{2}\sigma_{a_c}}\right) \tag{A2}$$

where

$$\operatorname{erf}(s) = \frac{1}{\sqrt{\pi}}\int_{-s}^{s} e^{-t^2}\,\mathrm{d}t \tag{A3}$$

and ζ is a zero-mean Gaussian random variable:

$$\zeta \sim N(0, \sigma_{a_c}) \tag{A4}$$

The dependence of the gain L on σ_{a_c}/A_c is plotted in Fig. A1. It is apparent that as σ_{a_c} decreases, L increases to its maximum value of

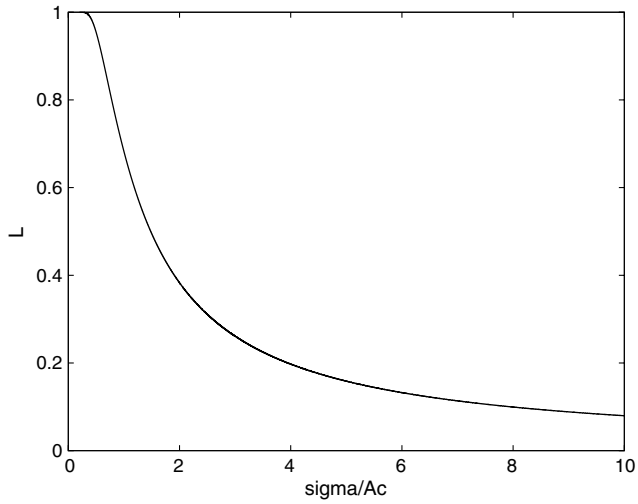

Fig. A1 RIDF corresponding to saturation.

one. An interesting alternative interpretation of L is available from Gokcek et al. [10], who state that L is equal to the probability of not reaching saturation.

In the derivation of the necessary conditions, the derivative of the RIDF is required. Differentiating Eq. (A2) with respect to s results in

$$\frac{\mathrm{d}\,\mathrm{erf}(s)}{\mathrm{d}s} = \frac{2}{\sqrt{\pi}} e^{s^2} \tag{A5}$$

so that

$$\frac{\mathrm{d}\,\mathrm{erf}^{-1}(\mathrm{L})}{\mathrm{d}L} = \frac{\sqrt{\pi}}{2} \exp\{[\mathrm{erf}^{-1}(L)]^2\} \tag{A6}$$

References

[1] Zarchan, P., *Tactical and Strategic Missile Guidance*, Vol. 124, Progress in Astronautics and Aeronautics, AIAA, Washington, D.C., 1990.

[2] Rusnak, I., "Advanced Guidance Laws for Acceleration Constrained Missile, Randomly Maneuvering Target and Noisy Measurements," *IEEE Transactions on Aerospace and Electronic Systems*, Vol. 32, No. 1, Jan. 1996, pp. 456–464. doi:10.1109/7.481287

[3] Gutman, S., *Applied Min-Max Approach to Missile Guidance and Control*, Vol. 209, Progress in Astronautics and Aeronautics, AIAA, Reston, VA., 2005.

[4] Hexner, G., and Shima, T., "Stochastic Optimal Control Guidance Law with Bounded Acceleration," *IEEE Transactions on Aerospace and Electronic Systems*, Vol. 43, No. 1, Jan. 2007, pp. 71–78. doi:10.1109/TAES.2007.357155

[5] Hexner, G., Shima, T., and Weiss, H., "LQG Guidance Law with Bounded Acceleration Command," *IEEE Transactions on Aerospace and Electronic Systems*, Vol. 44, No. 1, Jan. 2008, pp. 77–86. doi:10.1109/TAES.2008.4516990

[6] Gelb, A., and Vander Velde, W. E. V., *Multiple-Input Describing Functions and Nonlinear System Design*, McGraw–Hill, New York, 1968.

[7] Zarchan, P., "Complete Statistical Analysis of Nonlinear Missile Guidance Systems: SLAM," *Journal of Guidance, Control, and Dynamics*, Vol. 2, No. 1, 1979, pp. 71–78. doi:10.2514/3.55834

[8] Singer, R. A., "Estimating Optimal Tracking Filter Performance for Maneuvering Targets," *IEEE Transactions on Aerospace and Electronic Systems*, Vol. 6, No. 4, 1970, pp. 473–483. doi:10.1109/TAES.1970.310128

[9] Fitzgerald, R. J., "Shaping Filters for Disturbances with Random Starting Times," *Journal of Guidance, Control, and Dynamics*, Vol. 2, No. 2, 1979, pp. 152–154. doi:10.2514/3.55851

[10] Gokcek, C., Kabamba, P. T., and Meerkov, S. M., "An LQR/LQG Theory for Systems with Saturating Actuators," *IEEE Transactions on Automatic Control*, Vol. 46, No. 10, 2001, pp. 1529–1542. doi:10.1109/9.956049

[11] Bryson, A. E., and Ho, Y. C., *Applied Optimal Control*, Blaisdel, Waltham, MA, 1969.

[12] Jacobson, D. H., and Mayne, D. Q., *Differential Dynamic Programming*, Elsevier, New York, 1970.